AAPM 2021

JULY 25–29 | VIRTUAL

63RD ANNUAL MEETING & EXHIBITION

Using the Planning CT Scan for Pixel-To-Pixel Corrections of Cherenkov Intensity for Dose Imaging

[1]R. Hachadorian, [1,2]D. Alexander, [3]E. Chen, [1,4]D. Gladstone, [4]G. Gill, [1,2]M. Jermyn, [1,4]R. Zhang, [1,2]P. Bruza, [1,4]L. Jarvis, [1,2,4]B. Pogue.

1 Dartmouth College, Hanover NH, USA

2 DoseOptics LLC, Lebanon NH, USA

3 Dartmouth-Hitchcock Medical Center – Cheshire, Keene, NH, USA

4 Dartmouth-Hitchcock Medical Center / Norris Cotton Cancer Center, Lebanon, NH, USA

DARTMOUTH ENGINEERING 1867

CENTER FOR IMAGING MEDICINE AT DARTMOUTH

Dartmouth-Hitchcock NORRIS COTTON CANCER CENTER

AIM

To work toward the ability to monitor dose quantitatively using Cherenkov light. This requires correcting for tissue optical properties. We propose that the planning CT can be used to correct for the differences in tissue density, which is among the most substantial of attenuators.

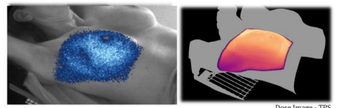

Dose Image - TPS

1. Small Feature Correction
   - Areola/Nipple
   - Blood/Vasculature
   - Surgical Scars
   - Curvature, Patient Geometry

2. Large-Scale Tissue Correction
   - Absorption/Scattering Properties of the tissue itself.
   - Overall Skin Pigment.

Video 1: Tissue optical properties can be divided into several categories. The goal is to achieve linearity with dose.

INTRODUCTION

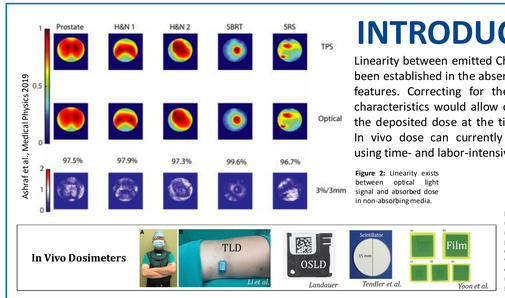

Linearity between emitted Cherenkov light has been established in the absence of attenuating features. Correcting for these features and characteristics would allow clinicians to know the deposited dose at the time of treatment. In vivo dose can currently only be realized using time- and labor-intensive dosimeters.

Figure 2: Linearity exists between optical light signal and absorbed dose in non-absorbing media.

Figure 3: Dosimeters currently utilized for in vivo dose measurements involve time to place and to process. Imaging dose with intensified cameras would offer a means of obtaining dose information remotely and require less processing.

METHODS

The CT scan is rendered as an isosurface, and normal vectors are generated at every surface vertex. The directionality of each vector is reversed and CT# is sampled along multiple locations up to 5 mm into the tissue. That average is projected onto the patient volume, translated to the perspective of the Cherenkov camera, registered to the patient background image, and masked using the Cherenkov light field. (Patients consented through IRB-approved study.)

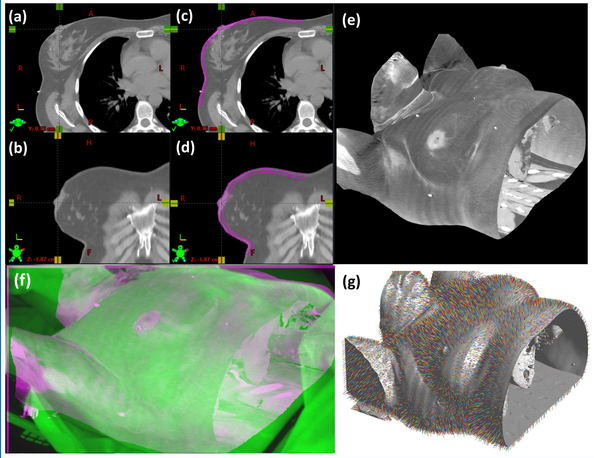

Figure 4: (a)-(d) differences in fibroglandular to adipose tissue are apparent. The magenta outline indicates the region sampled (where only the surface is relevant for Cherenkov dosimetry). (e) the rendered CT scan is used to co-register to the background image from treatment (f). (g) shows the map of surface normal vectors prior to sampling.

RESULTS

The spatial mapping of the CT scan enabled a pixel-by-pixel correction of the Cherenkov image. This improved the standard deviation over the means (σ/μ) of light output per unit dose by roughly 12%-13%. Light to dose linearity (R^2) increased by anywhere from 17% to 28%, depending on evaluation of beam energy and entrance or exit beam.

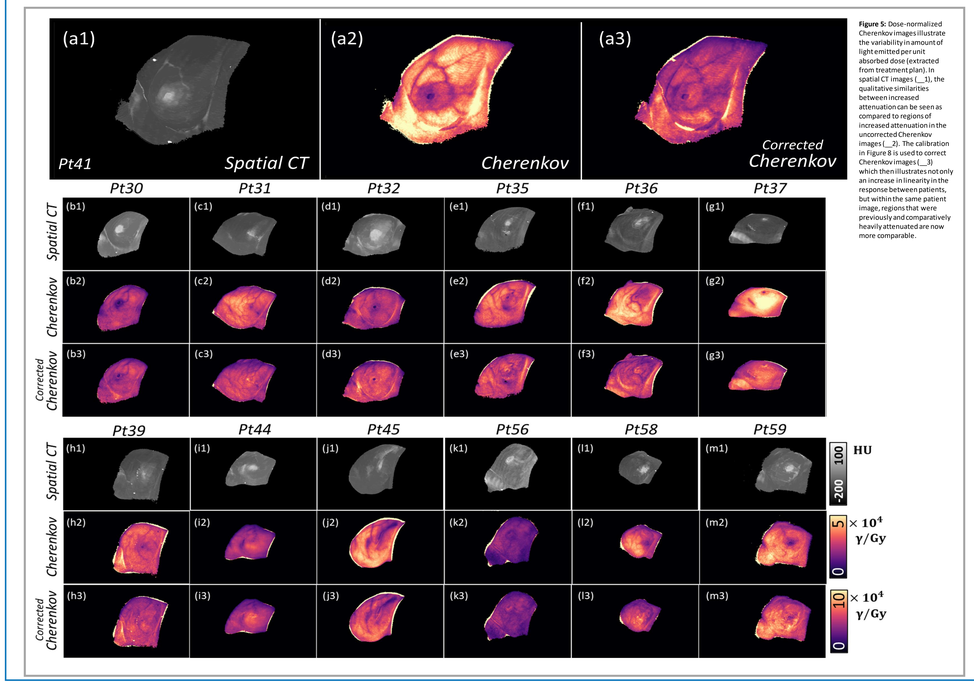

Figure 5: Dose-normalized Cherenkov images illustrate the variability in amount of light emitted per unit absorbed dose (extracted from treatment plan). In spatial CT images (_1), the qualitative similarities between increased attenuation can be seen as compared to regions of increased attenuation in the uncorrected Cherenkov images (_2). The calibration in Figure 8 is used to correct Cherenkov images (_3) which then illustrates not only an increase in linearity in the response between patients, but within the same patient image, regions that were previously and comparatively heavily attenuated are now more comparable.

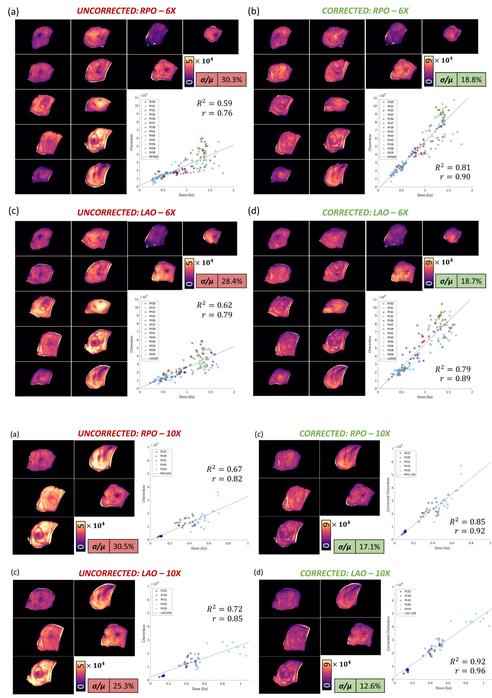

Figure 6: The calibration in Figure 8 is used to establish the relationship between the corresponding Cherenkov light output and average CT# (HU). Using this information, linear correction factors are computed (Equation 1) and assigned to each pixel in the original (not dose-normalized) images. In (a) the uncorrected entrance beam images are shown for 6 MV beam energies, with the computed standard deviation over the mean (or coefficient of variation (COV) expressed as percent), along with the linear fit R^2. In (b) there are notable improvements in the COV and the R^2 for the corrected images. Subfigures (c) and (d) mimic (a) and (b), respectively, and differ only in that they present exit beam data, for which notable improvements are also observed.

Equation 1 : The corrected, dose-normalized Cherenkov light intensity $I_{corr,D}(E)$ can be realized by taking the product between the simple multiplicative correction factor $c(HU(x,y),E)$ with the uncorrected intensity $I_{uncorr,D}(E)$. Fitting parameters A, b, C, D are listed below in Figure 8. A normalization CT# endpoint of -135 HU was selected as this represented a very low-density breast tissue which is unlikely to be extended beyond.

$$I_{corr,D}(E) = I_{uncorr,D}(E) \cdot c(HU(x,y),E)$$
$$= I_{uncorr,D} \cdot \left[\frac{A \cdot e^{b(-135)} + C \cdot e^{d(-135)}}{A \cdot e^{b(HU)} + C \cdot e^{d(HU)}}\right], \quad (1)$$

Figure 8: The calibration is generated by sampling over 20 ROI's for each patient, 10 corresponding to regions of very little, feature-based attenuation (light gray points), and 10 corresponding to regions of much attenuation (e.g. areola, surgical scar, prominent blood vessels, dark gray points). The resulting function is a summed exponential which appears to have continuity despite the dramatically reduced signal. In (a), this is shown for images recorded at 6 MV beam energies, and in (b), for 10 MV imaged treatments. Fitting parameters and goodness of fits are shown adjacent to each respective calibration.

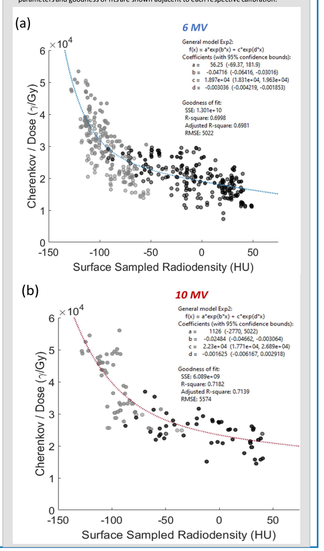

FUTURE WORK

In future work, we aim to couple inter-patient tissue optical property corrections with additional corrections to address inter-fractional changes, mostly pertaining to erythemic skin irritation.

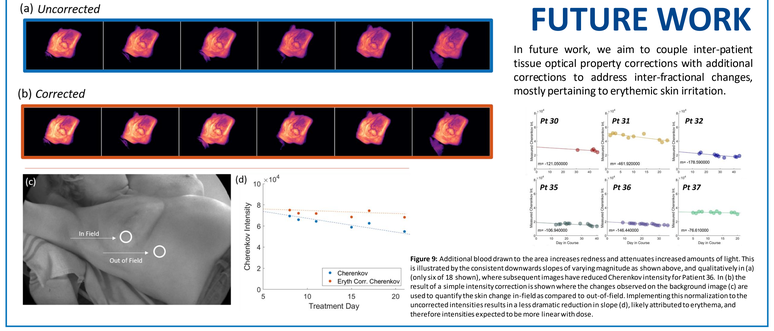

Figure 9: Additional blood drawn to the area increases redness and attenuates increased amounts of light. This is illustrated by the consistent downwards slopes of varying magnitude as shown above, and qualitatively in (a) (only six of 18 shown), where subsequent images have reduced Cherenkov intensity for Patient 36. In (b) the result of a simple intensity correction is shown where the changes observed on the background image (c) are used to quantify the skin change in-field as compared to out-of-field. Implementing this normalization to the uncorrected intensities results in a less dramatic reduction in slope (d), likely attributed to erythema, and therefore intensities expected to be more linear with dose.

REFERENCES

[1] L. A. Jarvis et al., "Cherenkov video imaging allows for the first visualization of radiation therapy in real time," International Journal of Radiation Oncology* Biology* Physics, vol. 89, no. 3, pp. 615–622, 2014.

[2] L. A. Jarvis et al., "Initial Clinical Experience of Cherenkov Imaging in External Beam Radiation Therapy Identifies Opportunities to Improve Treatment Delivery," International Journal of Radiation Oncology* Biology* Physics, 2020.

[3] P. J. Black, C. Velten, Y.-F. Wang, Y. Ni, Na, and C.-S. Wuu, "An investigation of clinical treatment field delivery verification using cherenkov imaging: IMRT positioning shifts and field matching," Medical physics, vol. 46, no. 1, pp. 302–317, 2019.

[4] T. Miao et al., "Cherenkov imaging for linac beam shape analysis as a remote electronic quality assessment verification tool," Medical physics, vol. 46, no. 2, pp. 811–821, 2019.

[5] X. A. Li et al., "Patterns of Failure Observed in the 2-Step Institution Credentialing Process for NRG Oncology/Radiation Therapy Oncology Group 1005 (NCT01349322) and Lessons Learned," Practical radiation oncology, vol. 10, no. 4, pp. 265–273, 2020.

[6] G. Ezzell et al., "Common error pathways seen in the RO-ILS data that demonstrate opportunities for improving treatment safety," Practical radiation oncology, vol. 8, no. 2, pp. 123–132, 2018.

[7] A. K. Glaser, R. Zhang, S. C. Davis, D. J. Gladstone, and B. W. Pogue, "Time-gated Cherenkov emission spectroscopy from linear accelerator irradiation of tissue phantoms," Optics letters, vol. 37, no. 7, pp. 1193–1195, 2012.

[8] R. Hachadorian et al., "Correcting Cherenkov light attenuation in tissue using spatial frequency domain imaging for quantitative surface dosimetry during whole breast radiation therapy," Journal of biomedical optics, vol. 24, no. 7, p. 071609, 2018.

[9] A. A. Oraevsky, S. L. Jacques, and F. K. Tittel, "Measurement of tissue optical properties by time-resolved detection of laser-induced transient stress," Applied optics, vol. 36, no. 1, pp. 402–415, 1997.

[10] A. Dimofte et al., "Determination of tissue optical properties in PDT treated head and neck patients," in Photonic Therapeutics and Diagnostics X, 2014, vol. 8926, p. 892624C.

[11] F. Bevilacqua, D. Piguet, P. Marquet, J. D. Gross, B. J. Tromberg, and C. Depeursinge, "In vivo local determination of tissue optical properties: applications to human brain," Applied optics, vol. 38, no. 22, pp. 4939–4950, 1999.

[12] M. Meinhardt, R. Krebs, A. Anders, U. Heinrich, and H. Tronnier, "Wavelength-dependent penetration depths of ultraviolet radiation in human skin," Journal of biomedical optics, vol. 13, no. 4, p. 044030, 2008.

[13] A. Kim, M. Khurana, Y. Moriyama, and B. C. Wilson, "Quantification of in vivo fluorescence decoupled from the effects of tissue optical properties using fiber-optic spectroscopy measurements," Journal of biomedical optics, vol. 15, no. 6, p. 067006, 2010.

[14] B. C. Wilson, "Measurement of tissue optical properties: methods and theories," in Optical-thermal response of laser-irradiated tissue, Springer, 1995, pp. 233–303.

[15] R. Hachadorian, P. Bruza, M. Jermyn, D. Gladstone, B. Pogue, and L. Jarvis, "Imaging radiation dose in breast radiotherapy by x-ray CT calibration of Cherenkov light," Nature communications, vol. 11, no. 1, pp. 1–9, 2020.

[16] L. Wang, A. J. Cmelak, and G. X. Ding, "A simple technique to improve calculated skin dose accuracy in a commercial treatment planning system," Journal of applied clinical medical physics, vol. 19, no. 2, pp. 191–197, 2018.

[17] T. J. Pfefer et al., "Reflectance-based determination of optical properties in highly attenuating tissue," Journal of Biomedical Optics, vol. 8, no. 2, pp. 206–215, 2003.

Funding: This work has been funded by grant R01 EB023909 from the National Institutes of Health, with hardware support through R44 CA232879 and with the support of the Norris Cotton Cancer Center shared resources in P01 CA023108.

Disclosures: L.A.J. and B.W.P. have a financial interest in DoseOptics, which manufactures cameras used in this study and is funded by SBIR grants; they also have a conflict of interest management plan at Dartmouth College and Dartmouth-Hitchcock Medical Center, which includes an independent review of the research integrity before publication. L.A.J. has a patent pending (application no. 62/874,124). R.L.H. has a patent pending (application no. 62/874,124). M.J. and P.B. are employees of DoseOptics. I.I.T. has a patent issued (WO/2019/165196). M.J. has a patent (WO 2019/143972 A2) pending to Dartmouth/DoseOptics LLC. P.B. has patents pending (62/967,302; 62/873,155; PCT/US19/14242; and PCT/US19/19135). D.J.G. has a patent issued (US10,201,718 B2, 2/12/2019). B.W.P. has patents (US 10201718 B2 and US 9731150 B2) issued to DoseOptics LLC and a patent (WO 2019/143972 A2) pending to Dartmouth/DoseOptics LLC. The remaining authors reported no disclosures or conflicts of interest.

CONTACT INFORMATION

Rachael Hachadorian, PhD: Rachael.L.Hachadorian.TH@dartmouth.edu

Prof. Brian W. Pogue, PhD (PI): Brian.W.Pogue@dartmouth.edu